

Obstacles to quantum annealing in a planar embedding of XORSAT

Pranay Patil,¹ Stefanos Kourtis,¹ Claudio Chamon,¹ Eduardo R. Mucciolo,² and Andrei E. Ruckenstein¹

¹*Department of Physics, Boston University, 590 Commonwealth Avenue, Boston, Massachusetts 02215, USA*

²*Department of Physics, University of Central Florida, Orlando, Florida 32816, USA*

We introduce a planar embedding of the k -regular k -XORSAT problem, in which solutions are encoded in the ground state of a classical statistical mechanics model of reversible logic gates arranged on a square grid and acting on bits that represent the Boolean variables of the problem. The special feature of this embedding is that the resulting model lacks a finite-temperature phase transition, thus bypassing the first-order thermodynamic transition known to occur in the random graph representation of XORSAT. In spite of this attractive feature, the thermal relaxation into the ground state displays remarkably slow glassy behavior. The question addressed in this paper is whether this planar embedding can afford an efficient path to solution of k -regular k -XORSAT via quantum adiabatic annealing. We first show that our model bypasses an avoided level crossing and consequent exponentially small gap in the limit of small transverse fields. We then present quantum Monte Carlo results for our embedding of the k -regular k -XORSAT that strongly support a picture in which second-order and first-order transitions develop at a finite transverse field for $k = 2$ and $k = 3$, respectively. This translates into power-law and exponential dependences in the scaling of energy gaps with system size, corresponding to times-to-solution which are, respectively, polynomial and exponential in the number of variables. We conclude that neither classical nor quantum annealing can efficiently solve our reformulation of XORSAT, even though the original problem can be solved in polynomial time by Gaussian elimination.

I. INTRODUCTION

Boolean satisfiability problems form an important subset of computer science problems which have been studied extensively with regard to their general solvability. These problems usually comprise of finding a set of bits, each of which can take values of either 0 or 1, which satisfy the set of constraints demanded by the particular problem. One of the simplest examples of such a constraint satisfaction problem is XOR-satisfiability, where each constraint (or clause) reads in a set of bits and requires their sum modulo 2 to be 0 or 1. A bit assignment (arrangement of 0's and 1's) which satisfies all the clauses in an XORSAT problem is said to be a solution.

Connections between such computer science (CS) problems and statistical physics models of bits (spins) is an active area of research. The generic approach encodes the solution of the computational problem in the ground state of a statistical mechanics model. This line of research has led to novel insights and algorithms, such as simulated annealing and belief propagation [1–3], which have become standard tools in many applied science areas. A shortcoming of most implementations of this approach is that the underlying physical systems tend to display glass transitions that prevent one from reaching the ground state, thus blocking the path-to-solution for the computational problem. While one may be tempted to connect the complexity of the computational problem to the glassiness of the model, this naive expectation is misdirected. A glass transition, and thus a barrier to solution, also occurs in some of the current statistical mechanics realizations of XORSAT, an “easy” computational problem in class P [4].

In a set of recent publications [5, 6] we introduced a planar embedding of universal classical computation which displays no finite temperature bulk phase transitions, thus eliminating an obvious obstruction to reaching solution through thermal annealing. In spite of this conceptual simplification, within our mapping the difficulty is transferred to the dynamical behavior as one cools to low temperatures. We find that, even

for some simple computational problems (such as multiplication) and 3-regular 3-XORSAT, a problem which is solvable in polynomial time by Gaussian elimination [7], the relaxation times into the ground state and thus the times-to-solution are extremely long. The source of glassiness in our reformulation of these easy computational problems can be traced back to two qualitatively different mechanisms. In the case of multiplication, a single thermally excited defect created in the annealing process translates into a macroscopic number of computational errors [6]. On the other hand, for 3-regular 3-XORSAT our statistical mechanics representation involves partial knowledge of input/output boundaries (see Appendix). For this “mixed-boundary conditions” case we have shown [5] that thermal annealing is an ineffective way of reaching solution (i.e., of determining the full state of the boundaries).

In this paper, we explore the alternative of employing quantum adiabatic annealing (QAA) [8–13] to solve our planar model of XORSAT efficiently. Specifically, we are motivated to ask whether our reformulation, which removes the first-order thermal transition, also removes the first-order quantum phase transition that was encountered in the original quantum annealing formulation of XORSAT on random regular graphs [9]. We present quantum Monte Carlo results for our embedding of the k -regular k -XORSAT. In particular, we study the nature of the phase transition along the quantum axis as a function of transverse field for $k = 2$ and $k = 3$. The first obstruction one could encounter in approaching the classical ground state along the quantum axis is an avoided level crossing, resulting in an exponentially small gap in the limit of small transverse fields and signaling an exponentially long time to solution [14]. We show that our embedding does not suffer from this avoided crossing shortcoming.

The $k = 2$ case is simple and can be solved via both thermal and quantum annealing. In particular, the $k = 2$ model displays a second-order phase transition along the quantum axis, corresponding to a time-to-solution that scales polynomially with the system size. In contrast, our results show that the

$k = 3$ model undergoes a first-order transition at a finite transverse field. This translates into an exponential scaling of energy gaps and thus to a time-to-solution that scales exponentially with the number of variables in the XORSAT instances. Thus, even though our embedding bypasses two of the obvious obstructions to annealing into the ground state — the classical phase transition at finite temperature along the classical axis and the perturbation theory collapse for small transverse field along the quantum axis — our results for $k = 3$ reinforce the conclusion that both classical and quantum annealing can be ineffective pathways to solution even for easy (i.e., complexity P) computational problems. The same conclusion was reached by Farhi *et al.* [9], whose approach also bypassed the “perturbation theory collapse” of Ref. 14 but not the thermodynamic transition along the classical axis. In summary, our embedding of classical computational problems into statistical mechanics models defines a class of systems with short-range interactions and no classical bulk thermal phase transitions that display slow glassy dynamics in both thermal and quantum annealing.

The outline of the paper is as follows. In Sec. II we provide an introduction to quantum annealing in the context of the general class of problems we are interested in studying, along with a comparison to simulated annealing. This is followed by Sec. III where we describe the particular problem we study and its lattice embedding that we investigate for efficiency of annealing. In Sec. IV we provide an interpretation for the efficacy of simulated annealing in reaching solutions in two classes of regular XORSAT problems, as well as weak perturbation theory argument concerning quantum annealing at small transverse fields. Sec. V presents numerical results from quantum Monte Carlo for a simple illustrative example of a single CNOT gate and builds on these results to address the more complex case of $k = 2, 3$ regular XORSAT through similar simulations. We present our conclusions in Sec. VI.

II. QUANTUM ADIABATIC ANNEALING ALGORITHM: OUTLINE AND GENERAL CONSIDERATIONS

The quantum adiabatic annealing (QAA) algorithm was introduced as a method to solve computational problems in Refs. [9, 15]. It exploits long-range quantum coherence in a time dependent quantum system whose defining Hamiltonian interpolates adiabatically between two limits. The goal is to use QAA to reach the ground state of a complicated classical Hamiltonian H , which encodes the solution of the computational problem at hand, by adiabatically deforming the quantum ground state of a “simpler” initial Hamiltonian, which is easy to prepare.

Concretely, a computational problem on N Boolean variables is mapped to a Hamiltonian H that describes interactions between N classical Ising spin degrees of freedom $\sigma_i^z = |\uparrow\rangle, |\downarrow\rangle$ for $i = 1, \dots, N$. The spin-up state $\sigma_i^z = |\uparrow\rangle$ can be chosen to represent bit state $x_i = 1$ and the spin-down state $\sigma_i^z = |\downarrow\rangle$ the bit state $x_i = 0$. The mapping is such that the bit assignment that corresponds to the ground-state spin configuration of H encodes the solution of the computational

problem. (Here we will mainly concern ourselves with a class of problems that have a single solution, such that the ground state of H is non-degenerate.)

In the QAA algorithm, the classical spins (bits) are represented by quantum spin-1/2 degrees of freedom. The QAA protocol is typically carried out at zero temperature and proceeds by preparing the system in a uniform superposition of all σ_i^z eigenstates by applying a strong transverse field (σ_i^z is a Pauli matrix that defines a local quantization axis for the i -th spin). Annealing is implemented by adiabatically “turning off” the transverse field while “turning on” the Hamiltonian H . This process defines a time-dependent Hamiltonian

$$H_a = (1 - s)H - sV, \quad (1)$$

where $V = \sum_{i=1}^N \sigma_i^x$ is the transverse field term and $s = f(t)$ is a time-dependent parameter. The protocol usually starts with $f(0) = 1$ to ensure that the system is in the transverse-field ground state, where each spin is polarized along the x -axis, and ends with $f(T_f) = 0$, which recovers the target Hamiltonian at time T_f . The quantum adiabatic theorem [16, 17] guarantees that the system remains in its instantaneous ground state if $f(t)$ varies “slowly enough” with time. To be more specific, it says that the total duration T_f of the protocol should satisfy

$$T_f \gg \hbar \frac{\max_s |V_{10}(s)|}{(\Delta E_{\min})^2}, \quad (2)$$

where $V_{m0} = \langle 0 | \partial H_a / \partial s | m \rangle$ in the eigenbasis spanned by $|m\rangle$, $m = 1, \dots, 2^N - 1$, and ΔE_{\min} is the minimum gap between the ground state and the first excited state encountered during the entire protocol.

Generally, V_{m0} is proportional to system size for a local Hamiltonian and the scaling of T_f is controlled by the scaling of the minimum gap. This implies that if the system passes through a phase transition where the gap vanishes, the time to solution using a quantum annealing protocol can be polynomial or exponential in system size depending on the behavior of the minimum gap with system size. Continuous phase transitions have a scale-invariant critical point, which implies that the gap must have a polynomial dependence on system size [18]. First-order transitions, on the other hand, manifest themselves in finite-size systems via gaps that vanish exponentially with system size, although there are pathological cases where the gap closing is only polynomial [19]. It is therefore highly probable that the QAA algorithm fails to find the solution when the annealing protocol described by H_a leads through a first-order transition in the thermodynamic limit.

In what follows, we will rewrite H_a as

$$H_a = JH - hV, \quad (3)$$

allowing J and h to take arbitrary positive values, to conform with common notation in the literature.

Since H is classical, one may also consider using simulated annealing (SA) to reach its ground state. In this protocol, $h = 0$ and one slowly varies the temperature T from $T = \infty$

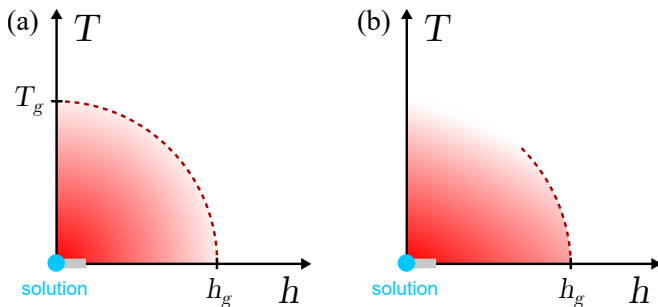


FIG. 1. Cartoon phase diagrams in the temperature-transverse field parameter space for two scenarios that may occur in the application of the SA and QAA algorithms to the solution of computational problems. In the scenario of panel (a), SA meets a transition to a glassy phase at $T = T_g$, whereas QAA encounters a first-order quantum phase transition at $h = h_g$. An example of this scenario is the 3-XORSAT problem, as it was formulated and studied in, e.g., Refs. 10 and 20. Dashed line indicates a putative phase boundary that terminates at the two critical points on the axes. Panel (b) depicts the scenario we introduce and study in this work, namely, the case where there is no bulk classical thermodynamic phase transition to a glass phase, but the obstruction of a first-order quantum phase transition nevertheless remains. An example of this scenario is the lattice embedding of 3-regular 3-XORSAT we introduce in Sec. III. The dashed line indicates a putative phase boundary that terminates at the quantum critical point, but does not extend all the way to the classical axis. In both panels, a thick grey line close to the origin delineates the range where the perturbative gap collapse argument of Ref. 14 is potentially relevant and may obstruct the QAA protocol.

to $T = 0$. Local thermal dynamics, implemented via, e.g., the Metropolis algorithm, progressively lead toward lower-energy configurations. SA, and in fact any local classical algorithm, fails whenever a first-order transition into a glass phase is encountered upon reducing the temperature. This is true regardless of the hardness of the computational problem encoded by H [4, 20].

When SA and QAA are taken on equal footing as methods for the solution of a given problem, they give rise to a phase diagram as a function of T and h , whose origin represents the solution of the problem. Fig. 1 shows two distinct scenarios for this phase diagram. In the first scenario, the solution is separated from both the classical high- T paramagnet and the strong-field quantum paramagnet, i.e., the initial states of the SA and QAA protocols, respectively, by first-order transitions. This is a commonly encountered scenario for computational problems, such as satisfiability or coloring, and is illustrated in Fig. 1(a). For example, the 3-regular 3-XORSAT problem, as it was formulated and studied in Ref. 10 and also briefly introduced below, belongs to this category.

In this work, we will use a lattice reformulation of computational problems that lacks the classical transition to a glassy phase. This formulation introduces an alternative scenario to the aforementioned one and raises the question of whether the quantum phase transition is absent as well in this case, i.e., whether the two transitions are somehow linked. Below we will provide evidence for a negative answer to this question: our results suggest that the quantum phase transition remains

present and first-order, and hence most probably accompanied by exponentially vanishing gaps in progressively larger finite-size systems, even in the absence of a thermodynamic classical transition to a glassy phase.

III. k -REGULAR k -XORSAT AND LATTICE EMBEDDING

A. The XORSAT problem

In this section, we describe the mapping of the the k -regular k -XORSAT problem [21] to a spin Hamiltonian. We choose XORSAT because it is a prototypical problem in both physics and theoretical computer science. Even though XORSAT can be solved in polynomial time with Gaussian elimination, it nevertheless has evaded efficient solution with any local algorithm, including variants of the Davis-Putnam algorithm [22], message-passing methods [23], stochastic search [24], simulated annealing [20], and quantum adiabatic annealing [10].

Here we focus on the k -regular variant of k -XORSAT. This constraint satisfaction problem is defined on N Boolean variables subject to N clauses, where each clause takes in k bits and each bit participates in k clauses. The solution to the problem is a bit assignment that satisfies all clauses. An XORSAT clause evaluates to 0 (false) or 1 (true) if the sum of the bits in the clause modulo 2 is 0 or 1, respectively. In spin language, this can be interpreted as requiring the product of the spins in a particular clause to be positive or negative and associating an energy cost to the unfavorable outcome. For example, the spin Hamiltonian can be written as

$$H = - \sum_{j=1}^N \prod_{i \in c_j} \sigma_i^z, \quad (4)$$

where c_j is the set of the k indices of the spins that participate in the j -th clause, for k odd. Since clauses are not constrained to connect nearby spins only, this spin Hamiltonian is best represented as a bipartite k -regular graph, where one independent set of vertices represents the spins and the other the clauses. A random instance of this problem is thus a randomly generated bipartite k -regular graph. A solution of an instance (if it exists) is given by a corresponding ground state of H .

Numerical examination of the QAA algorithm for Hamiltonian (4) restricted to $k = 3$ and to instances with unique ground states showed that the minimum gap closes exponentially with system size, indicating a first-order transition at a particular value of the transverse field in the thermodynamic limit [10]. This finding implies that QAA takes an exponentially long time to find the solution in this formulation of 3-regular 3-XORSAT. On the other hand, application of the SA algorithm to the XORSAT problem reveals a random first-order transition into a glassy phase at some characteristic temperature — see, e.g., Ref. 20. These results suggest that the solutions of XORSAT instances reside deep inside a glass phase and are inaccessible to both classical local search algorithms and QAA, despite the fact that XORSAT is computationally tractable (i.e., in complexity class P).

B. Lattice embedding

In an attempt to avoid the aforementioned obstructions to the solution of XORSAT, here we introduce a lattice embedding of the problem that circumvents the classical thermodynamic transition. The idea is based on previous works by some of us [5, 6]. Note that this lattice embedding does not enable an efficient solution of the problem via SA, despite the absence of the glass transition, as the dynamics instead becomes glassy upon approaching $T = 0$. The rationale for this reformulation is rather to see whether the avoidance of the thermodynamic glass transition and hence the absence of a finite- T classical glass phase has any effect on the quantum axis.

The lattice embedding is achieved by drawing each variable and each clause as a bit line or “bus” and laying all lines on a 2D plane, with vertical lines corresponding to clauses and horizontal ones to variables, as shown in Fig. 2. Each variable (clause) corresponds to a horizontal (vertical) Ising spin chain and the intersection between variable chains and clause chains is mediated by CNOT or SWAP gates. If the y -th variable participates in the x -th clause, then a CNOT gate is placed at the intersection of the x -th vertical line with the y -th horizontal line, else a SWAP gate is placed to ensure that the bit and clause do not couple.

Each gate has two inputs (i_1 and i_2) and two outputs (o_1 and o_2). The gate constraints can be written in spin language as

$$H_{x,y}^0 = -\sigma_{x,y;i_1}^z \sigma_{x,y;o_1}^z - \sigma_{x,y;i_2}^z \sigma_{x,y;o_2}^z \quad (5a)$$

for a SWAP gate and

$$H_{x,y}^1 = -\sigma_{x,y;i_1}^z \sigma_{x,y;o_1}^z + \sigma_{x,y;i_2}^z \sigma_{x,y;o_2}^z \quad (5b)$$

for a CNOT, where the subscripts x and y specify the position of each gate. To accommodate the y -th variable to appear negated in the x -th clause, we can simply change the sign of the second term in (5b). Here we will deal only with monotone instances where no variables appear negated, and hence no such change will be necessary.

Inter-site ferromagnetic bonds of strength J are placed between the outputs of a gate and the inputs of nearest-neighbor gates. This construction ensures that when all ferromagnetic bonds are satisfied by a spin configuration, the corresponding bit assignment satisfies all clauses and is the solution to the problem. The overall spin Hamiltonian is

$$H = - \sum_{\langle x,y;x',y' \rangle} \sum_{v=1,2} \sigma_{x,y;o_v}^z \sigma_{x',y';i_v}^z + g \sum_{x,y} H_{x,y}^{A_{x,y}} \quad (5c)$$

$$- \sum_x (\sigma_{x,0;o_2}^z \sigma_{x,\partial_y=0}^z + \sigma_{x,N;i_2}^z \sigma_{x,\partial_y=N}^z) \quad (5d)$$

$$+ g \sum_x (\sigma_{x,\partial_y=0}^z \pm \sigma_{x,\partial_y=N}^z). \quad (5e)$$

The sums are over $x, y = 1, \dots, N$, so that a problem instance with N variables maps to a lattice with N^2 sites with a gate at each site, $\langle \dots \rangle$ denotes neighboring positions on the lattice,

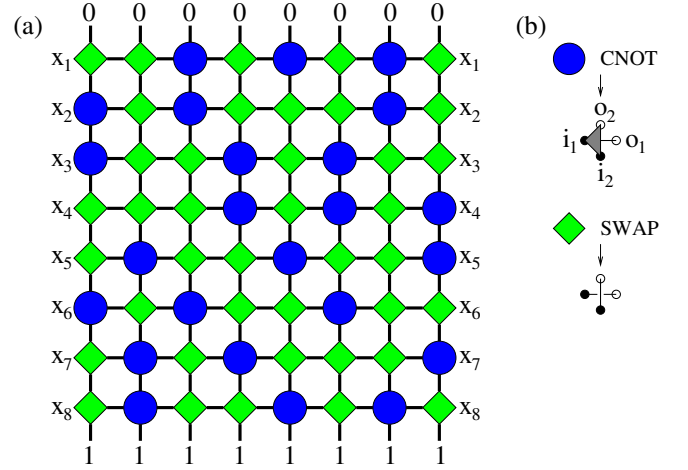


FIG. 2. (a) Lattice representation of 3-regular 3-XORSAT instance with 8 variables and 8 clauses as a 8×8 lattice of CNOT and SWAP gates. There are 4 bits coupled by a gate at each position of the lattice, as shown in (b). The variable bits x_i record the solution of the problem upon termination of a protocol that reaches the ground state. Upper and lower boundary states are forced by a strong field that favors the uniform bit states shown. (b) Sketch of couplings between bits in each of the gates. Lines denote ferromagnetic bonds in the spin representation and grey triangle represents the 3-spin term in Eq. (5b). The formula for the 3-XORSAT instance shown here is $(x_2 \oplus x_3 \oplus x_6) \wedge (x_5 \oplus x_7 \oplus x_8) \wedge (x_1 \oplus x_2 \oplus x_6) \wedge (x_3 \oplus x_4 \oplus x_7) \wedge (x_1 \oplus x_5 \oplus x_8) \wedge (x_3 \oplus x_4 \oplus x_6) \wedge (x_1 \oplus x_2 \oplus x_8) \wedge (x_4 \oplus x_5 \oplus x_7)$.

v is the orientation of the bond labeled as 1 (2) for horizontal (vertical), and g is a constant that offsets the energy cost of the gate and boundary terms with respect to the bond terms.

The first line of Eq. (5c) defines the interactions in the bulk. A is the adjacency matrix of the bipartite k -regular graph that defines the problem instance, as described above. When $A_{x,y} = 1$, a CNOT gate is placed at position (x, y) , otherwise a SWAP is placed there instead, as sketched in Fig. 2. Note that in our convention indexing proceeds from left to right and top to bottom. We consider the limit $g \rightarrow \infty$, so that outputs are essentially “dummy” spins, whose state is completely controlled by the gate inputs. When the ground state of H is reached, the solution appears on the left and right boundaries of the lattice, which are left free. The requirement that clauses sum modulo 2 to 0 or 1 is enforced by the term on the last line, which acts only on the top and bottom rows of boundary spins and whose relative sign between top and bottom depends on whether k is odd or even. For example, for $k = 2$ we choose + (all-zeros state in bottom row) to ensure that all clauses sum modulo 2 to 0, whereas for $k = 3$ we choose - (all-ones state in bottom row), which requires all clauses to sum modulo 2 to 1. When $g \rightarrow \infty$ this interaction becomes a hard constraint. This clause constraint is then propagated to the bulk by the terms in Eqs. (5d) and (5e), which define the interaction between spins at the top ($\partial_{y=0}$) and bottom ($\partial_{y=N}$) boundaries and bulk gate spins.

Here we restrict our analysis to instances of k -regular k -XORSAT which have all the minimum nonzero number of solutions. For $k = 3$, generic problems with a unique solution

exist. For all such problems, a spin reversal transformation exists which maps the solution to the all spins down state [10] and we shall assume that our system has already undergone this transformation. We will focus on these problems below, as they are a finite fraction of all 3-XORSAT instances and are thus good representatives of the full ensemble [25]. For $k = 2$, there are always two solutions, one of which corresponds to the all-down state.

We generate 3-regular 3-XORSAT instances with unique solutions by first generating a random bipartite 3-regular graph and retaining only those instances which have an odd determinant, as this condition enforces a unique solution [7]. We also ensure that the generated graph is connected. We then use the adjacency matrix of this graph to define the lattice embedding. For the k -regular variants of XORSAT, the finite lattices are by definition square. Varying the clause-to-variable ratio amounts simply to changing the lattice aspect ratio.

IV. ANALYTIC RESULTS: LIMITING CASES AND WEAK-FIELD PERTURBATION THEORY

A. Dilute constraint limit and 2-XORSAT

In the lattice setup, if we only have SWAP gates at all the intersections between clauses and bits, then we recreate disconnected transverse field Ising chains. This can be seen by considering the action of the SWAP gate as given in Eq. (5a), where we see that spins are only coupled along either the horizontal or vertical directions. Considering also the transverse-field term, and remembering that input and output spins of gates are locked when $g \rightarrow \infty$, the Hamiltonian for a decoupled chain reduces to

$$H_a = -J \sum_{i=1}^N \sigma_i^z \sigma_{i+1}^z - h \sum_{i=1}^N \sigma_i^x, \quad (6)$$

where i now denotes the coordinate along the chain. This is simply the transverse-field Ising (TFI) chain, which is known to have a continuous phase transition at $h = J$ and a critical behavior which is well understood [26]. This would then imply that in the limit of zero CNOT gates on the lattice, we would have a second-order transition characterized by the TFI chain universality class.

The lattices that arise in our embedding of k -regular k -XORSAT have k CNOTs in each vertical and horizontal line. This leads to a CNOT density $\frac{k}{N}$. For $N \gg k$, the system reduces to independent TFI chains coupled at a vanishing number of points. Two possibilities arise for a potential phase transition that the system may undergo as a function of h . The first is that the phase transition remains continuous as for decoupled TFI chains when the density of ‘‘impurities’’ is vanishing. The second possibility is that this vanishing number of impurities drastically changes the nature of the phase transition from continuous to first-order. In the first case, we would be left with a lattice which is able to solve the computational problem in polynomial time. In the second case, the lattice would

require exponential time and would be an example of a system where adding a vanishing number of impurities changes the order of the transition. An example of this behavior occurs in the polymerization of rubber [27], where the process of vulcanization leads to a vanishing number of cross-links between polymers, which in turn changes the state of rubber from liquid to solid.

Let us examine the $k = 2$ case. Each instance contains a periodic Ising chain, as it corresponds to a series of ferromagnetic bonds between spins, where each spin participates in only two bonds, as illustrated in Fig. 3(a). This lattice can be reconfigured as an Ising chain with offshoots, as shown in Fig. 3(b), using the following ‘‘unraveling’’ procedure. First, pick an arbitrary CNOT and an arbitrary direction (vertical or horizontal), then draw a link between the starting CNOT and its neighbor in that direction. As there is only one neighbor in either direction, there is no ambiguity in this step. Now rename the neighbour as the starting site and follow the same procedure using the direction perpendicular to the current direction. This process creates a unique loop with spin chains branching out at the locations with CNOTs. This equivalence is valid as SWAP gates only braid chains over each other without interactions. Taking the limit of large size, we would expect the average separations between CNOTs to be of order N and the fluctuations about this should be statistically small.

Examining the energetics of domain walls in this system illustrates why SA is expected to be efficient in reaching the solution in this case. Let us consider a configuration of this system with a number of domain walls which would correspond to a typical state encountered at finite temperature, as seen in Fig. 3(b). If we translate a domain wall through a CNOT, it generates two domain walls on the other side, one of which can be healed by translating it out to the boundary, while the other can travel around the ring until it meets another domain wall, with which it can mutually annihilate. In this way, domain walls can be healed all the way to a state without domain walls, i.e. the ground state, in a smooth sequence of steps that monotonically reduce energy other than the one additional bond that must be broken when passing through a CNOT. In Sec. V, we will show that 2-XORSAT is also efficiently solved with QAA.

We now apply the same argumentation to the lattice representation of the $k = 3$ case. We decompose the lattice into a loop using the unraveling procedure. Fig. 4 shows a realization of 3-regular 3-XORSAT with the same backbone structure as Fig. 3. The additional CNOT gates now provide frustrating interactions which force the backbone chain to have all spins pointing down and spin inversion symmetry for that section of the lattice is lost. We can look at this in detail using the particular cross-connecting CNOT shown in Fig. 4 (highlighted in red) for the classical ground state where all bonds must be satisfied. If we assume that the spins lying in the blue chain are +1, then spin A3 would be forced to -1, implying B1 has to be -1. From this it follows that B2 must be +1, as B3 is +1 due to a direct connection to the boundary. This would then force B4 and as a result C2 to be +1. And as C3 is +1 due to the boundary, C1 must both be -1 creating a contradiction as C1 belongs in the blue chain and must be +1. In

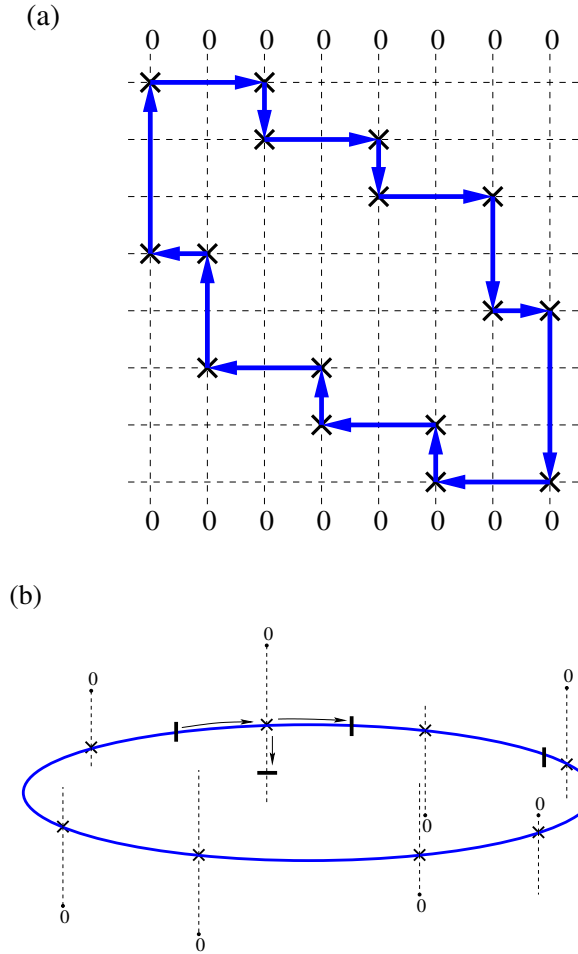


FIG. 3. (a) “Backbone” loop for a $k = 2$ instance of k -regular k -XORSAT in the lattice representation. SWAP gates are omitted and CNOT gates are denoted by \times symbols. Arrows indicate the “unraveling” procedure described in the text. (b) The corresponding unraveled loop picture with spin chains radiating out of CNOT gates. Domain walls are sketched as $|$ symbols and their movement, indicated by the arrows, heals broken bonds and reduces energy.

terms of the ring structure in Fig. 4(b), this would mean cross-connections between various offshoots, which would destroy the one-dimensional nature of the chain.

The convoluted loop structure of $k = 3$ instances implies that domain wall movement now becomes highly non-trivial: we cannot simply heal domain walls by moving them to the boundary, but must instead translate them to the next CNOT, where they can perhaps annihilate by merging with another domain wall. However, moving a domain wall around the ring now produces a large number of domain walls, as each CNOT results in branching. Each of the resulting defects can be healed only after traversing half the ring on average. This illustrates why SA will fail to solve this problem efficiently, even though our lattice formulation can be shown to feature no thermodynamic glass transition [5, 6] and is also found to be similar to the vertex models proposed in Ref. 5 (see also Appendix A).

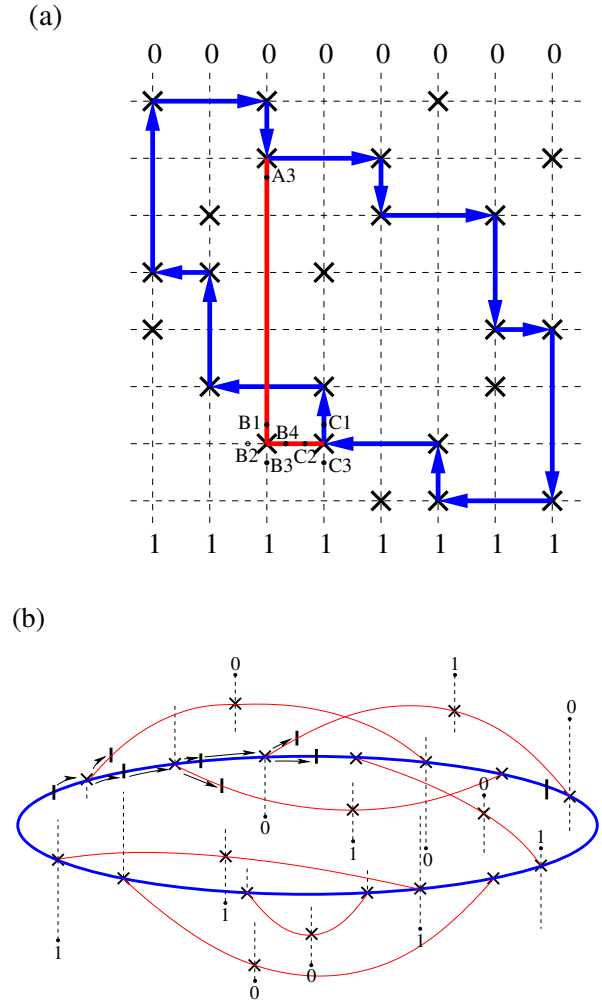


FIG. 4. (a) Lattice representation of 3-regular 3-XORSAT instance with the same backbone as the one shown in Fig. 3(a). The backbone cannot independently fluctuate between positive and negative values, due to constraining couplings to spins outside the backbone (example shown in red), and hence the backbone cannot be isolated as in the $k = 2$ case. (b) Loop equivalent for the $k = 3$ realization, with arrows showing domain wall movement that in this case involves branching of domain walls at CNOT gates.

B. Weak-field perturbation theory: absence of gap collapse

Altshuler *et al.* [14] pinpointed a potential setback inherent in the QAA protocol. Perturbative analysis showed that generic classical Hamiltonians set up to solve computational problems may give rise to an avoided level crossing when an arbitrarily small transverse field is added. This implies an exponential reduction in annealing velocity, in order to maintain fidelity with the target ground state. In order to fully address the potential issue of avoided level crossings and to show that it is not present in our lattice formulation, we will now present a full perturbative treatment of the general k -regular k -XORSAT problem. A similar analysis appears in Ref. 28.

Consider the spectrum of a classical spin model that represents a computational problem. We again restrict ourselves

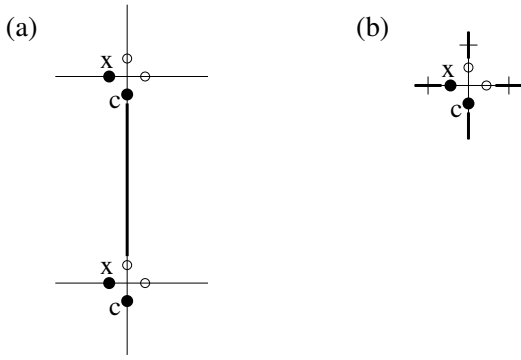


FIG. 5. (a) Sketch of y -bond connecting the spins of two gates. The state of this bond only affects the four perturbation correction terms corresponding to the spins shown as filled circles. (b) Flipping the control spin (X) of a CNOT gate switches the state of the bonds marked with a cut. Along the vertical line, either the upper or lower bond can be broken (upper bond shown here).

to instances with a unique solution. The ground state of the model is therefore unique. The first excited state is degenerate and is made out of all those configurations that differ from the ground state in the status of a single bond. At $h = 0$, the corresponding energy levels have a difference of J from the ground-state level. Altshuler *et al.* show that perturbative corrections to the gap between the ground state and the first excited state for small h should depend on system size in the general case, an argument resulting from the disorder present in most spin representations of computational problems. This leads to a second-order correction proportional to Nh^2 , where N is the system size. They conclude that for arbitrarily small h there exists N such that the correction surpasses J , leading to an avoided level crossing.

Contrary to the above argument, we will show that there are no vanishing gaps in the weak-field limit for k -regular k -XORSAT. First, let us define a bond to have two states, the set state where it is satisfied and the broken state, and the two inputs of a gate to be degrees of freedom (as mentioned in the previous section, the outputs of the gates are completely determined by the inputs, so they are not degrees of freedom, and thus will be ignored). Each gate has four bonds radiating out. Flipping either of the two input spins of a SWAP gate flips the states of two bonds, irrespective of what their states are and irrespective of what the state of the spin was. For the CNOT gate, flipping the carry input (C) switches the state of two bonds, but flipping the control input (X) switches the state of three bonds, again irrespective of the initial bit states (Fig. 5). Flipping a boundary spin switches the state of only one bond. The important thing to note here is that the cost induced due to a flip does not depend on the states of spins. Therefore, perturbation theory on the ground state creates N corrections, but none of these depend on the ground-state configuration.

First, consider that all excited-state levels are non-degenerate. This situation is artificial and we treat it only because it simplifies the discussion of the physically relevant case of highly degenerate excitation manifolds discussed be-

low. The excitation energy E_i^{flip} of the state created due to a single spin flip at site i is one of $J, 2J, 3J$, depending on whether it belongs to the boundary, a SWAP gate or a CNOT gate respectively. The second-order perturbation correction to the ground-state energy is

$$\Delta E^{(0)} = \sum_{i=1}^N \frac{h^2}{E_i^{\text{flip}}} \propto \frac{Nh^2}{J}, \quad (7)$$

so far in accordance with the Altshuler *et al.* argument. Any term in this sum is determined only by the state of the four bonds radiating out of a particular point on the lattice and the gate corresponding to that point. Each lattice point carries two spins, implying that the status of a particular bond, which can only control two lattice points, is relevant only to at most four terms in this sum. As the only difference between the ground state and one of the first excited states is the status of one bond, only four or lesser number of terms in the perturbation corrections for both states can differ. It follows that the change in the gap due to these corrections is

$$|\Delta E^{(0)} - \Delta E^{(1)}| \propto h^2/J, \quad (8)$$

which is *independent* of system size, similar to the clean TFI model [29].

We now take into account the mixing of the degenerate first-excited states amongst themselves due to the transverse field. This typically results in the degenerate levels spreading over a band of width $\propto h$ and is, once again, independent of system size. After first-order degenerate perturbation theory, the states that result from the mixing of the first-excited configurations at zero field are

$$|\tilde{E}^{(l)}\rangle = \sum_i \alpha_i^{(l)} |E_i^{(1)}\rangle, \quad (9)$$

where $|E_i^{(1)}\rangle$ is a first-excited configuration with energy $E^{(1)}$. The states $|\tilde{E}^{(l)}\rangle$ are then used to perform higher-order perturbation theory. Second-order corrections look like

$$\Delta \tilde{E}^{(l)} = h^2 \sum_{i,j} \sum_m \frac{\alpha_i^{(l)} \alpha_j^{(l)}}{|E^{(1)} - E_m|} \langle E_i^{(1)} | V | m \rangle \langle m | V | E_j^{(1)} \rangle, \quad (10)$$

where m runs over states that are necessarily not $|E_i^{(1)}\rangle$. Of the ‘‘diagonal’’ terms $|\langle E_i^{(1)} | V | m \rangle|^2$, at most four are nonzero, by the same reasoning we employed above. For the terms with $i \neq j$, if $|E_i^{(1)}\rangle$ has a frustrated bond in the bulk, there is no way to connect it to $|E_j^{(1)}\rangle$ via V using states $|m\rangle$ within the first level. On the other hand, when $|E_i^{(1)}\rangle$ contains a frustrated boundary bond, we can connect to all other such singly excited states. However, these second-order processes are equally possible for all states, regardless of gate configuration, and hence this correction amounts to a uniform shift of all levels. The above means that the relative shift of a first-excited state level with respect to the ground-state level is going to be bounded in the same way as it was for

just one spin configuration in the first level. The same argumentation extends to higher corrections straightforwardly. We therefore conclude that there is no perturbative gap collapse in the weak-field limit for the models we study here.

We remark that the arguments presented above also extend to the random graph spin model for 3-regular 3-XORSAT studied in Ref. 10, and evidence for this can be seen in the duality of $h \leftrightarrow J$ that that model possesses. This duality implies that the spectrum is identical for $h \leftrightarrow J$, and as the strong transverse field limit has a well defined gap, the ferromagnetic limit does too.

V. NUMERICAL RESULTS

In this Section, we apply the QAA protocol to the lattice models for k -regular k -XORSAT we introduced above. We simulate QAA via projector Quantum Monte Carlo (QMC) simulations to investigate the transitions encountered upon varying the transverse field. Our calculations are set up following the style of simulations for TFI models [30, 31] due to the similarity in the Hamiltonians and they are able to access ground state expectation values for various observables. It is known that for glassy systems or at first-order transitions, this style of QMC suffers from long equilibration times and non-ergodic behavior [32]. Cluster updates using larger objects made out of multiple spins, which have been found to be useful for particular frustrated Ising antiferromagnets [33], were found to be rejection-prone for our 3-XORSAT model due to the three-body terms that make up CNOTs. This limits the sizes of the lattices we can simulate and also how deep our simulations can reach into the ferromagnetic phase. We use a variety of local and replica exchange updates [34, 35] to speed up the algorithm. Details of the implementation of the replica exchange method can be found in Ref. 35, where it has been applied to a similar model. We will study our models in the context of continuous and first-order phase transitions, which show a diverging and a finite correlation length, respectively. The energy gap is expected to close for both types of transitions, but the scaling of the minimum gap with system size differs, closing as $\sim N^{-\gamma}$ for the former and $\sim e^{-N^\gamma}$ for the latter ($\gamma > 0$).

The lattice models of k -regular k -XORSAT with a transverse field, defined by Eqs. (3) and (5), show two phases: a disordered phase in the limit of strong transverse field and an ordered phase in the ferromagnetic (or classical) limit. To simplify our analysis, we set $h = 1$ and vary J through the transition between the two phases. To find the critical value of the ferromagnetic coupling J_c and the nature of the phase transition, we use the Binder cumulant [36]

$$U_m = \frac{3}{2} \left(1 - \frac{1}{3} \frac{\langle M_z^4 \rangle}{\langle M_z^2 \rangle^2} \right), \quad (11)$$

where M_z is the magnetization of the system in the z direction. In the strong transverse field limit, the system is magnetized along the x axis, which implies that $M_z = 0$, whereas in the ferromagnetic limit all spins are aligned, leading to a saturation of magnetization. U_m is defined such that it evaluates

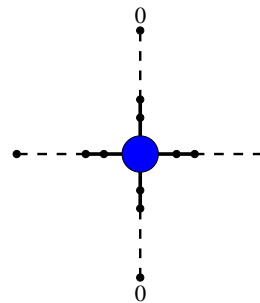


FIG. 6. Illustration of two TFI chains coupled at their center by a CNOT gate. The boundary spins of the vertical chain are fixed.

to zero in the disordered phase and unity in the ordered one. At the phase transition, U_m goes from 0 to 1 within a window of J that gets narrower as system size increases. For a continuous transition, the behavior is monotonically increasing in most cases, although exceptions are known [37], and for a first-order transition U_m has a negative peak at the critical point which diverges with system size as L^d , where d is the dimensionality of the system [38].

The Binder cumulant is chosen here to be sensitive to Z_2 symmetry breaking, which would be the symmetry usually studied in Ising systems. For the $k = 3$ case, the boundary conditions enforce a single solution, meaning that the system is not doubly degenerate and in this case, U_m shows a non-zero value on the disordered side before the transition (seen in Fig. 9), as the histogram favors net negative magnetization. This anomaly is also seen in the transverse field Ising chain with fixed boundary conditions similar to the ones studied.

We begin our study of the effectiveness of QAA on 2-regular 2-XORSAT by first applying the algorithm to the building block of this system: a single CNOT gate coupling long spin chains, as shown in Fig. 6. The CNOT coupling is expected to result in no drastic change to the continuous phase transition of the two chains, as it is a single defect in a large system. Numerical evidence for this is shown in Fig. 7. Even for large systems of two chains intersecting, the magnetization histogram shows no coexistence of phases, indicative of a second-order transition. For first-order transitions, on the other hand, the same histogram would show a bimodal distribution, indicative of phase coexistence [38]. We expect the same conclusion to extend to the case of a large number of these “cross”-linked chains connected horizontally when the separation between CNOT gates is large, which is the case for $k = 2$, as shown in Fig. 3. It is seen that CNOTs interact only along a linear chain and correlation length growth is controlled by the physics of the TFI chains connecting them. We therefore expect a continuous phase transition at $h \sim J$.

We analyze 2-XORSAT instances by studying the behavior of U_m and the evolution of the magnetization histograms – see Fig. 8. 20 realizations are used for each size and the critical value of J is found to be close to unity, which matches the decoupled TFI chain value. For $k = 2$, the two ground states correspond to the configuration with all spins pointing down and the configuration with all bit line spins pointing up and a complicated ordering of the clause spins which is consistent

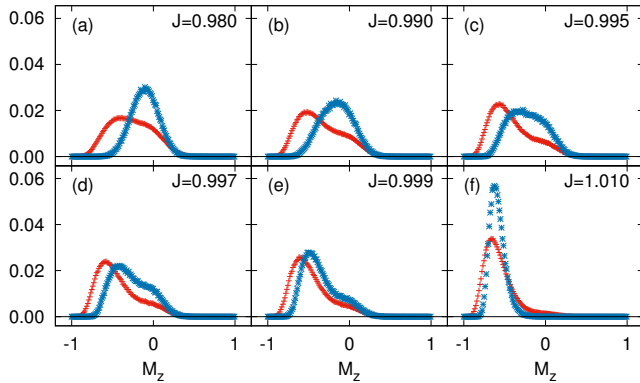


FIG. 7. Magnetization histograms for the transverse field system shown in Fig. 6 with 81 spins per chain (crosses) and 321 spins per chain (stars), as obtained from QMC calculations at $h = 1$. As J increases (a-f), the average magnetization switches values without developing a strong double peak structure even for large size.

with the solution and realization dependent. Due to the non-trivial structure of the ground states, U_m has to be defined using only the variable spins, as they form a spin-symmetric subset. This implies that the order parameter we use for U_m is the average z -magnetization squared of only the row spins i_1 and o_1 at each (x, y) position, which make up half of the total spins. For all the realizations of all lattice sizes, we found that U_m never becomes negative and the magnetization histograms show no sign of phase coexistence, indicating a continuous transition, as seen in Fig. 8.

The QAA protocol for 3-regular 3-XORSAT proceeds in the same vein as for $k = 2$. Using QMC simulations, we study the Binder cumulant using the full magnetization (as $k = 3$ has only one ground state) as a function of ferromagnetic coupling J for lattice sizes ranging from 6×6 to 16×16 . For each lattice size, we study 20 realizations of the 3-regular 3-XORSAT on the lattice with unique solutions. We find that for most of the realizations and for all sizes the Binder cumulant shows a negative peak. This can be seen in Fig. 9(g) for all realizations of a 16×16 lattice. Due to lack of ergodicity typically seen at first order phase transitions, we had to reject a large number of QMC simulations, retaining only those where both phases are represented as some simulations are not able to break out of the paramagnetic phase. This in itself only indicates that we may have a first-order transition but does not say so definitively. Showing that the negative peak in the Binder cumulant scales as number of sites is taken to be definite proof that the system is undergoing a first-order transition but we are unable to perform this analysis due to insufficient data quality and range of sizes. We omit error bars in Figs. 8(g) and 9(g) for clarity and as the error bars are small compared to the spread of the Binder cumulant values for different realizations.

Fig. 9 shows the evolution of the histogram as a function of J for the 3-regular 3-XORSAT including the value of J at which U_m is found to be minimum. The histogram indicates

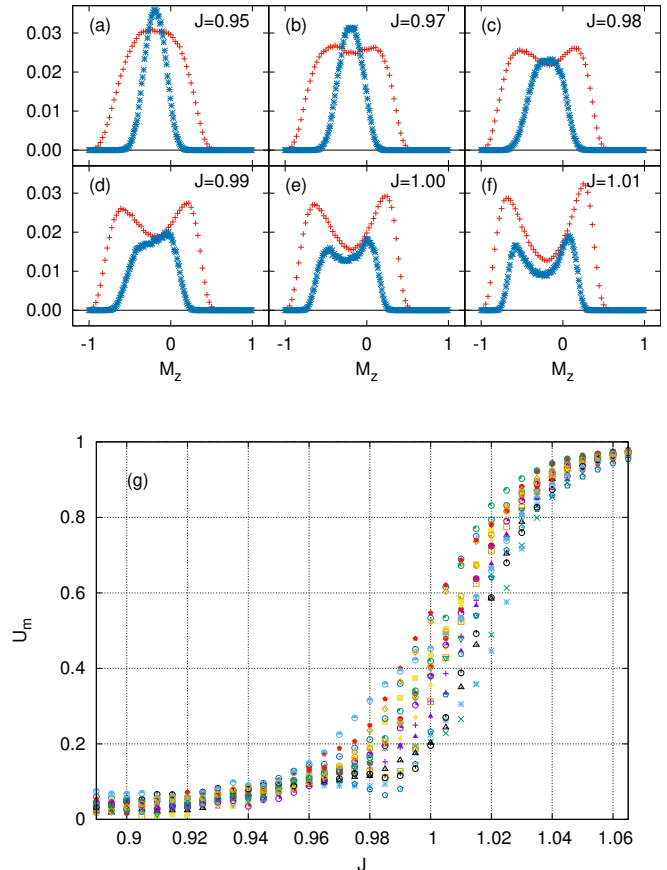


FIG. 8. (a-f) Magnetization histograms for a single realization of the 2-XORSAT lattice with size 6×6 (crosses) and another with size 16×16 (stars) for increasing J . The slight asymmetry in the two peaks of the histograms may be caused by non-ergodicity issues in the QMC simulation. (g) Binder cumulant for 20 realizations of size 16×16 . In all panels $h = 1$.

that there is a coexistence of phases which sharpens with increasing size and the phase transition can potentially develop into a first-order transition in the thermodynamic limit. Our system sizes and data quality limit our analysis, but for the system sizes we can access the first order nature appears to persist to the largest system size (Fig. 9). It is important to stress here that although the density of gates is vanishing in the thermodynamic limit, they are placed in a correlated manner, and can hence define the criticality of this model.

VI. SUMMARY AND CONCLUSION

We introduced a statistical mechanics representation of the XORSAT problem that recasts each instance as a planar grid of reversible gates acting on bits that represent the Boolean variables of the problem. The reason we chose this particular embedding of XORSAT is that it lacks a classical thermodynamic phase transition. We studied this system with quantum annealing and showed that it does not suffer from the

ACKNOWLEDGMENTS

We would like to thank Anders W. Sandvik and Jun Takahashi for suggesting improvements to the algorithms and sharing valuable technical expertise and Lei Zhang for valuable results from simulated annealing. We would also like to thank Chris Baldwin, Phillip Weinberg, and Itay Hen for useful discussions. The computational work was performed using the Shared Computing Cluster administered by Boston University’s Research Computing Services. We used QuSpin for checking the Quantum Monte Carlo simulation against exact diagonalization calculations [39]. This work was partially supported by the U.S. Department of Energy (DOE), Division of Condensed Matter Physics and Materials Science, under Contract No. DE-SC0019275 (PP, CC, and ERM).

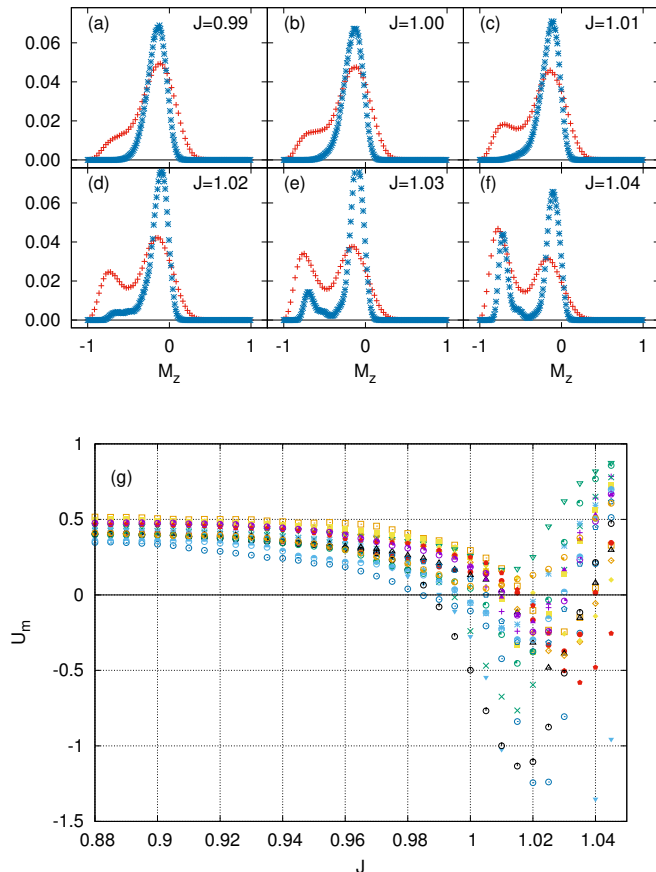


FIG. 9. (a-f) Magnetization histograms for a single realization of the 3-regular 3-XORSAT lattice with size 6×6 (crosses) and another with size 16×16 (stars) for increasing J . (g) Binder cumulant for 20 realizations of size 16×16 . In all panels $h = 1$.

perturbation theory collapse found by Altshuler *et al.* [14] at small transverse field strengths. We found that 3-regular 3-XORSAT displays a first-order transition at intermediate values of the transverse field, implying that quantum annealing leads to a time-to-solution that scales exponentially with the size of the system. Our results also suggest that the physics of the phase transition is determined not only by the density of CNOT defects, but also by their correlations. Taken together, these results on this alternative embedding of XORSAT reinforce the conclusion that both thermal and quantum annealing, which are intrinsically local approaches, can be inefficient in solving even simple problems (in computational complexity class P).

Appendix A: Mapping to the vertex model

Here we comment on the limitation of using thermal annealing to reach the ground state of 3-regular 3-XORSAT in spite of the absence of a bulk thermodynamic phase transition [5]. The simplest way to understand the slow thermal relaxation into the ground state of the XORSAT model is to use the recipe of Ref. 5 to embed XORSAT into the alternative spin model shown in Fig. 10. In this model, only half the boundary spins are fixed in each boundary, corresponding to the clause spins being fixed by a strong field in Eq. (5e), with the free bits (spins) on the rest of the boundaries. Reaching the ground state of this model through thermal annealing requires that information propagates between the boundaries until all free spins on both boundaries are fixed. This “mixed boundary condition” case in which only partial initial information is available on the input/output boundaries was already studied in Ref. 5. There it was found that thermal annealing is ineffective in reconciling the non-local information between the two boundaries, explaining the slow relaxation of the lattice embedding of 3-regular 3-XORSAT.

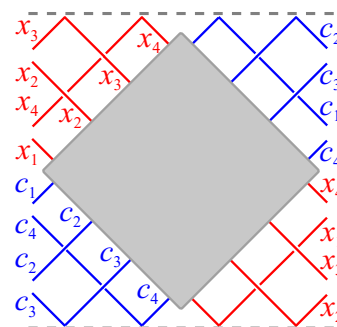


FIG. 10. Illustration of the mapping of the lattice formulation of k -XORSAT onto the general vertex model framework for computational problems introduced in Ref. 5, here shown for a 4×4 lattice. The grey shaded area is the placeholder in which a lattice like the one shown in Fig. 2(a) plugs into after a 45° rotation. In this embedding, clause bits (blue) are fixed and variable bits (red) are left free at both left and right boundaries, whereas all bit lines are “reflected” at the top and bottom boundaries (dashed lines).

-
- [1] S. Kirkpatrick, C. D. Gellat Jr., and M. P. Vecchi, *Science* **220**, 671 (1983).
- [2] M. Mézard, G. Parisi, and R. Zecchina, *Science* **297**, 812 (2002).
- [3] M. Mézard and A. Montanari, *Information, physics, and computation* (Oxford University Press, 2009).
- [4] F. Ricci-Tersenghi, *Science* **330**, 1639 (2010).
- [5] C. Chamon, E. R. Mucciolo, A. E. Ruckenstein, and Z.-C. Yang, *Nat. Commun.* **8**, 15303 (2017).
- [6] L. Zhang, S. Kourtis, C. Chamon, E. R. Mucciolo, and A. E. Ruckenstein, preprint arXiv:1812.01621 (2018).
- [7] Y. Yang, *Math. Comput. Educ.* **47**, 224 (2013).
- [8] S. Boixo, *Nat. Phys.* **10**, 218 (2014).
- [9] E. Farhi, J. Goldstone, S. Gutmann, and M. Sipser, arXiv:quant-ph/0001106 (2000).
- [10] E. Farhi, D. Gosset, I. Hen, A. W. Sandvik, P. Shor, A. P. Young, and F. Zamponi, *Phys. Rev. A* **86**, 052334 (2012).
- [11] T. Kadowaki and H. Nishimori, *Phys. Rev. E* **58**, 5355 (1998).
- [12] T. Albash and D. A. Lidar, *Physical Review X* **8**, 031016 (2018).
- [13] E. Farhi, J. Goldstone, S. Gutmann, J. Lapan, A. Lundgren, and D. Preda, *Science* **292**, 472 (2001).
- [14] B. Altshuler, H. Krovi, and J. Roland, *Proc. Natl. Acad. Sci. USA* **107**, 12446 (2010).
- [15] E. Farhi, J. Goldstone, S. Gutmann, J. Lapan, A. Lundgren, and D. Preda, *Science* **292**, 472 (2001).
- [16] G. H. Wannier, *Physics Physique Fizika* **1**, 251 (1965).
- [17] T. Kato, *J. Phys. Soc. Japan* **5**, 435 (1950).
- [18] S. L. Sondhi, S. M. Girvin, J. P. Carini, and D. Shahar, *Rev. Mod. Phys.* **69**, 315 (1997).
- [19] C. R. Laumann, R. Moessner, A. Scardicchio, and S. L. Sondhi, *Phys. Rev. Lett.* **109**, 030502 (2012).
- [20] F. Ricci-Tersenghi, M. Weigt, and R. Zecchina, *Phys. Rev. E* **63**, 026702 (2001).
- [21] D. S. Johnson and M. R. Garey, **1** (1979).
- [22] H. Haanpää, M. Jarvisalo, P. Kaski, and I. Niemelä, *Journal on Satisfiability, Boolean Modeling and Computation* **2**, 27 (2006).
- [23] H. Jia, C. Moore, and B. Selman, in *Theory and Applications of Satisfiability Testing, 7th International Conference, SAT 2004* (2005) pp. 199–210.
- [24] M. Guidetti and A. P. Young, *Phys. Rev. E* **84**, 011102 (2011).
- [25] T. Jörg, F. Krzakala, G. Semerjian, and F. Zamponi, *Phys. Rev. Lett.* **104**, 207206 (2010).
- [26] P. Pfeuty, *Annals Phys.* **57**, 79 (1970).
- [27] P. J. Flory and J. Rehner Jr, *J. Chem. Phys.* **11**, 512 (1943).
- [28] S. Knysh and V. Smelyanskiy, arXiv:1005.3011 (2010), arXiv:1005.3011.
- [29] S. Suzuki, J.-i. Inoue, and B. K. Chakrabarti, *Quantum Ising phases and transitions in transverse Ising models*, Vol. 862 (Springer, 2012).
- [30] A. W. Sandvik, *Phys. Rev. E* **68**, 056701 (2003).
- [31] C.-W. Liu, A. Polkovnikov, and A. W. Sandvik, *Phys. Rev. B* **87**, 174302 (2013).
- [32] L. T. Brady and W. van Dam, *Phys. Rev. A* **93**, 032304 (2016).
- [33] S. Biswas and K. Damle, *Phys. Rev. B* **97**, 085114 (2018).
- [34] K. Hukushima and K. Nemoto, *J. Phys. Soc. Japan* **65**, 1604 (1996).
- [35] J. Takahashi and K. Hukushima, *Journal of Statistical Mechanics: Theory and Experiment* **2019**, 043102 (2019).
- [36] K. Binder, *Z. Phys. B Condens. Matter* **43**, 119 (1981).
- [37] S. Jin, A. Sen, and A. W. Sandvik, *Phys. Rev. Lett.* **108**, 045702 (2012).
- [38] K. Binder, *Rep. Progr. Phys.* **50**, 783 (1987).
- [39] P. Weinberg and M. Bukov, *SciPost Physics* **2**, 003 (2017).